

The infrared spectrum of massive protostars: circumstellar disks and high mass star formation Barr, A.G.

#### Citation

Barr, A. G. (2022, April 12). The infrared spectrum of massive protostars: circumstellar disks and high mass star formation. Retrieved from https://hdl.handle.net/1887/3283538

Version: Publisher's Version

Licence agreement concerning inclusion of doctoral

License: thesis in the Institutional Repository of the University

of Leiden

Downloaded from: <a href="https://hdl.handle.net/1887/3283538">https://hdl.handle.net/1887/3283538</a>

**Note:** To cite this publication please use the final published version (if applicable).

# 1 | Introduction

The quote at the start of this book expresses man's wonder at his place in the universe. It reveals how this wonder has existed for many years, the quote being taken from a poem written some 3000 years ago. Indeed humanity's curiosity towards the universe is evident from the earliest of discovered civilisations. The scale of the universe is so grand, and our occupation of it so small, that today it is scarcely possible not to have an increased sense of wonder in relation to the poem's author, as science unravels more and more of the mysteries surrounding the universe. But as more are resolved, yet more are revealed, and the wonder seems rather to increase than to disappear. From exoplanets that we can easily relate to, to clusters of galaxies and supermassive black holes, our little planet begins to feel rather insignificant; a small speck lost in a vast sea of strange and wonderful objects.

Closer to home, the ever increasing chemical complexity beheld e.g. the discovery of glycine on the comet 67-P/Churyumov-Gerasimenko, proves that there are many interesting puzzles that we can, quite literally, get our hands on. With continuously improving facilities and computational capabilities, astronomers have never been better equipped to answer all of the enthralling questions that the universe poses.

Centrally, the question as to our own origin has intrigued humanity for millennia. How did we get here? The chemical complexity observed in star forming regions presents the question: did these molecules have a role to play? Consequently understanding what the organic inventory of regions of planet formation is, and what are the processes involved in their formation, become key questions.

### 1.1 Star Formation

The formation of stars and planets is one of the key areas of modern day astronomy. Understanding how these objects came to be, which have been visible to humanity across all generations, is not as easy as it would seem to appear. The current understanding, which has come a long way in recent years, is that stars are born in cold, tenuous clouds of dust and gas called giant molecular clouds (GMCs) (Shu et al. 1987). As areas of these clouds become gravitationally unstable, they begin to collapse leading to increasing amounts of dust and gas infalling into a concentrated region called a pre-stellar core (Shu 1977). As this proceeds, the material begins to heat up, forming a protostar. At this point the star is still deeply embedded in the cloud which envelopes it in such a way that the star is invisible at optical wavelengths.

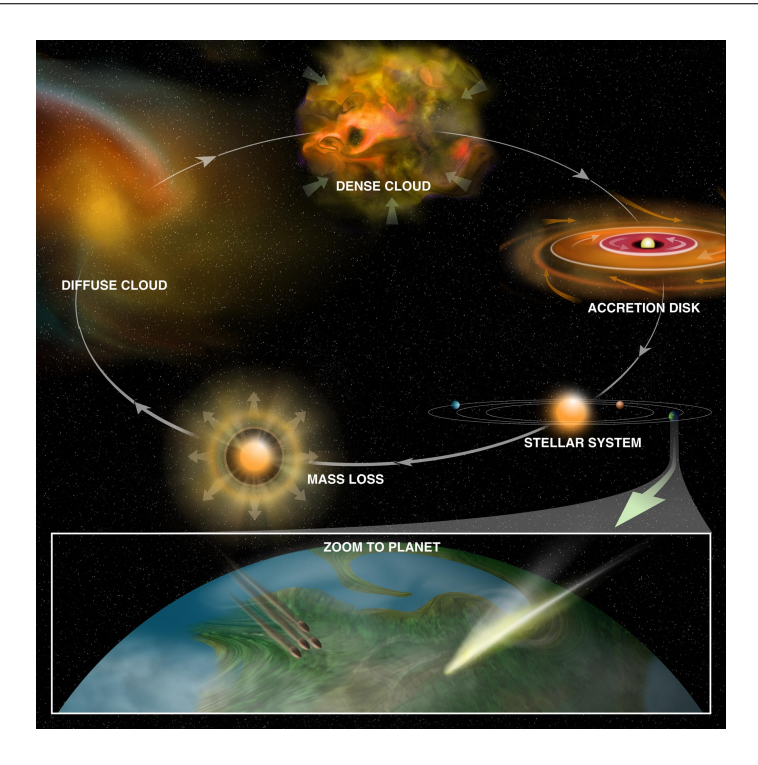


Figure 1.1: The life cycle of stars; from their birth in dense clouds to their death in supernovae. The planet formation process occurs during this cycle, extricably linking these two processes. The material dispensed in supernovae is recycled back into the surrounding cloud where it can once again be used for star formation. Acknowledgement: Bill Saxton (NRAO/AUI/NSF)

In Figure 1.1 we see that the next stage in the evolution involves a circumstellar disk, through which material can accrete onto the protostar, thus it increases in mass and continues to grow (Stahler & Palla 2005). The disk is a consequence of the conservation of angular momentum, as rotating, infalling material spreads out in a flattened structure around the star (Turner et al. 2014). Large outflows and winds perpendicular to the plane of the disk also form as material is ejected from the star-disk system; so the envelope and molecular cloud begin to be dispersed (Stahler & Palla 2005). While this takes place, dust in the disk agglomerates and begins to form planetesimals. Eventually these grow to larger and larger sizes, also acquiring the gas that is in the disk to eventually form planets, resulting in a stellar-planetary system. Eventually the star will begin to fuse hydrogen in its core and, after millions to billions of years, it will exhaust its supply of fuel and will die, shedding its outer layers back into the interstellar medium (Figure 1.1). And so the life cycle of the star is complete; the loop is closed, and the cycle repeats.

This general sequence of star formation does not apply equally to both low  $(M < 8M_{\odot})$  and high mass stars  $(M \ge 8M_{\odot})$ . The fusion of hydrogen in the core of massive stars occurs when the star is still deeply embedded in its envelope, whereas in low mass stars this occurs when the star reaches the main sequence (after  $\sim 5 \times 10^7$  yr)

1.1. STAR FORMATION 3

and the disk has been dispersed (after  $\sim 1 \times 10^7$  yr). Also planets have yet to be detected around O-type stars with the most massive host stars observed with a planet being 3-5  $M_{\odot}$ , and less discoveries are made as the stellar mass increases (Reffert et al. 2015; Grunblatt et al. 2019; Hollands et al. 2021). This likely reflects the short Kelvin-Helmholtz and disk dispersal timescales of massive stars compared to low mass stars, thus planets have much less time to form, as well as the high radiation fields of massive stars (Veras et al. 2020).

#### 1.1.1 Low Mass Star Formation

With this flavour of the star formation cycle, let us look more closely into the details of this complex process.

The GMCs in which stars form are gravitationally bound structures that exist within even larger clouds of HI gas in the cold interstellar medium (ISM), and range from  $>10^4~M_{\odot}$  up to  $10^7~M_{\odot}$ , observed in other galaxies (Vogel, Kulkarni & Scoville 1988; Sakamoto et al. 1999) and have densities of  $10^2$ - $10^3~\rm cm^{-3}$ . GMCs are turbulent and energy injection via internal and external mechanisms replenish this turbulence leading to support against gravitational collapse, and lifetimes estimated ranging from  $1\text{-}3\times10^7~\rm years$  (Krumholz, Matzner & McKee 2006).

Within GMCs, intricate cloud structure is observed in the form of web-like networks of filaments and fibres, formed through supersonic flows which compress the gas into either bound or unbound structures (André et al. 2014). Such structure is shown in Figure 1.2. Filaments can be from  $\sim 1$  pc to  $\sim 30$  pc in size and are significantly more dense compared to their environment. The distribution of filaments varies from cloud to cloud, and even within GMCs themselves, where the filaments are aligned in regions of high column density and more disorganised in regions of lower column density (Hill et al. 2011; Palmeirim et al. 2013). These are the sites of star formation where filaments gravitationally fragment into clumps and pre-stellar cores.

The cores can be either bound or unbound structures, with the most massive almost certainly bound (Bertoldi & McKee 1992). They are observed as local maxima in the column density distribution of filaments seen in submillimeter/millimetre continuum emission, or molecular species such as NH<sub>3</sub> and N<sub>2</sub>H<sup>+</sup>. Pre-stellar cores have subsonic turbulence and thermal motions that exceed non-thermal motions. There is a sharp transition however between the quiescent core and the gas in the surrounding cloud where the opposite is true, on scales of filament widths (0.1 pc) (Pineda et al. 2010). The cores are isothermal, of temperatures 10-20 K, and, being in an unstable hydrostatic equilibrium, eventually collapse forming a  $1/r^2$  density distribution, in the approximation of negligible turbulence (Hunter 1977; Shu 1977). Due to an increase in opacity, the core becomes adiabatic in the centre and eventually the collapse is halted in the innermost region where the temperature continues to rise. Once hydrogen fusion can begin, a zero-age main-sequence (ZAMS) star is formed.



Figure 1.2: Herschel image of the star forming region RCW106 in the Southern constellation of Norma, taken as part of Herschel's Hi-GAL key project. The three colours in the image correspond to 70  $\mu m$  (blue), 160  $\mu m$  (green) and 250  $\mu m$  (red). Very bright, young stars are illuminating the surrounding cloud causing dust radiation seen in these three colours. The powerful winds of these stars blow bubbles and excavate the surrounding cloud. Filamentary structures of dust and gas can be seen as web-like networks extending across the entire image. Stars are forming all along these filaments, which signify the densest regions of the cloud. Acknowledgement: UNIMAP / L. Piazzo, La Sapienza-Universitá di Roma; E. Schisano / G. Li Causi, IAPS/INAF, Italy)

1.1. STAR FORMATION 5

### 1.1.2 Circumstellar Disks

Disks are typically modelled as viscous fluids in which turbulence redistributes angular momentum (Shakura & Sunyaev 1973), rather than particle collisions, as in the case for a standard fluid. Loss of angular momentum is the driving force behind the evolution of the disk and occurs in the perpendicular direction to disk rotation. Conservation of angular momentum requires the spreading out of the disk, where most of the disk mass flows radially towards the star, and a small fraction of the disk mass carries angular momentum outwards, thus spreading out the surface density. This is predicted but has not yet been observed.

Disk evolution also occurs through disk winds. The presence of stellar magnetic field lines which thread the disk allow for a sufficiently ionised disk to form a magneto-hydrodynamic (MHD) disk wind, removing material from the disk. Magnetic tension and magnetic pressure gradients dominate the thermal pressure in a region above the disk surface and, in this way, disk winds can also remove angular momentum from the disk as the magnetic field exerts a torque on the disk while material that is accelerated along field lines gain angular momentum.

Powerful winds driven by the protostar result in the production of jets and outflows perpendicular to the disk axis. Jets have higher velocities than the outflows and are more collimated because they are primarily due to the stellar wind, whereas outflows consist of entrained material from the envelope that is swept up by the winds resulting in wide angles which surround the jet at the centre. In some cases, if the jet is powerful enough, it may drive the outflow. The launching point of the wind may vary radially from the star, with the launching point spread over a range of radii. Winds are thought to be magneto-centrifugally driven due to the presence of magnetic fields in circumstellar disks, thus driving MHD winds and jets. These come in the form of the disk wind model (see above) and X-wind model. X-winds are launched closer to the star compared to disk winds, with the possibility of both types being present driving different velocity components.

#### Disks in High Mass Young Stellar Objects

The role of disks in the process of massive star formation is a hotly debated topic (Beltrán & de Wit 2016). From a theoretical standpoint, some sort of non-spherical accretion is needed to overcome the strong stellar winds and radiation pressure from the star for it to continue growing, most likely in the form of a disk (Nakano 1989; Jijina & Adams 1996). However non-spherical accretion may also come in the form of multidirectional accretion flows for the more massive objects (Liu et al. 2015; Maud et al. 2017; Goddi et al. 2020). B-type sources are described as being scaled-up versions of their low mass counterparts in terms of the disk (Beltrán & de Wit 2016), however only a few examples of observations of very clear Keplerian disks around O-type stars stars are known, showing that stable disks can form around the most massive protostars but may be rare (Patel et al. 2005; Kraus et al. 2010; Johnston et al. 2015; Maud et al. 2019; Zapata et al. 2019). Protostars of mass > 30  $M_{\odot}$  typically show rotating non-equilibrium structures often named 'toroids', on scales of >1000 AU (Beltrán et al. 2005; Cesaroni et al. 2007). The lack of ubiquity of disks in massive young stellar objects (MYSOs) may be an observational bias as

massive stars lie systematically further away compared to low mass stars, therefore higher spatial resolution is required to detect these disks (milliarcsecond resolution is required to resolve these structures). Further evidence for disks comes from near infrared observations of CO emission in Keplerian rotation which derive very high temperatures (up to 4500 K) and column densities ( $\sim 10^{21}$  cm<sup>-2</sup>), consistent with the inner regions of a circumstellar disk (Bik & Thi 2004; Ilee et al. 2013). The question as to how massive stars actually form is still very much open, particularly for O-type stars above 30  $M_{\odot}$ , and much remains to be answered. Very high spatial resolution studies are required to properly address this and firmly establish the different accretion mechanisms of massive star formation.

#### 1.1.3 Massive Star Formation

While the mass distribution of galaxies necessitates that most stars that form will be low mass stars, massive stars have a far more significant role to play in the universe on galactic and extra-galactic scales, extending their influence to many different areas of astrophysics. The distribution of mass is described by the initial mass function, which is a probability distribution with a negative slope, stating that the number of stars in a given mass range decreases with mass. Visually, the very high ionising flux that comes from massive stars, and their strong winds, means that fantastic images of these star forming regions can be obtained, such as the Cygnus-X region, a large field of view image of which is shown in 1.3, where many different physical structures are formed. One of the massive stars central to this thesis, AFGL 2591, lies, impossible to discern, somewhere in this star forming region. Massive stars act simultaneously as catalysts and inhibitors of star formation, as stellar feedback both appeases and disrupts this process. Powerful winds and ionising gas from massive stars, and shocks from supernovae, sweep up material into dense shells, promoting further gravitational collapse to form new stars; these also disrupt molecular clouds injecting turbulence into quiescent clouds preventing the formation of new stars or dispersing them entirely. The strong radiation from massive stars also regulates the phases of the ISM via heating, ionisation and dissociation. Finally the enrichment of the ISM in atoms ranging in mass from carbon to rubidium is important with this being the sole production process for a handful of these elements. In this thesis we aim to shed some light onto how these important stars come to be, and the processes that occur during their formation.

A sequence of massive star formation can be made for high mass star formation, and is expected to span around 10<sup>5</sup> yr (Beuther et al. 2007). A cartoon illustration of the widely accepted process is given in Figure 1.4 and is based on Cesaroni et al. (2005b). High mass stars also are born in GMCs and they play an important role in the life cycle of GMCs where ionised hydrogen (HII) regions and outflows from OB associations can inject energy on large enough scales to support the clouds, however simultaneously, photoevaporation from HII regions is the dominant destruction mechanism (Zinnecker & Yorke 2007). Thus stellar feedback from massive stars is of fundamental importance to the galactic ecosystem on local scales. The pre-stellar cores of massive stars are themselves contained in infrared dark clouds (Rathborne, Jackson & Simon 2006) which are seen in absorption against mid-infrared continuum

1.1. STAR FORMATION 7

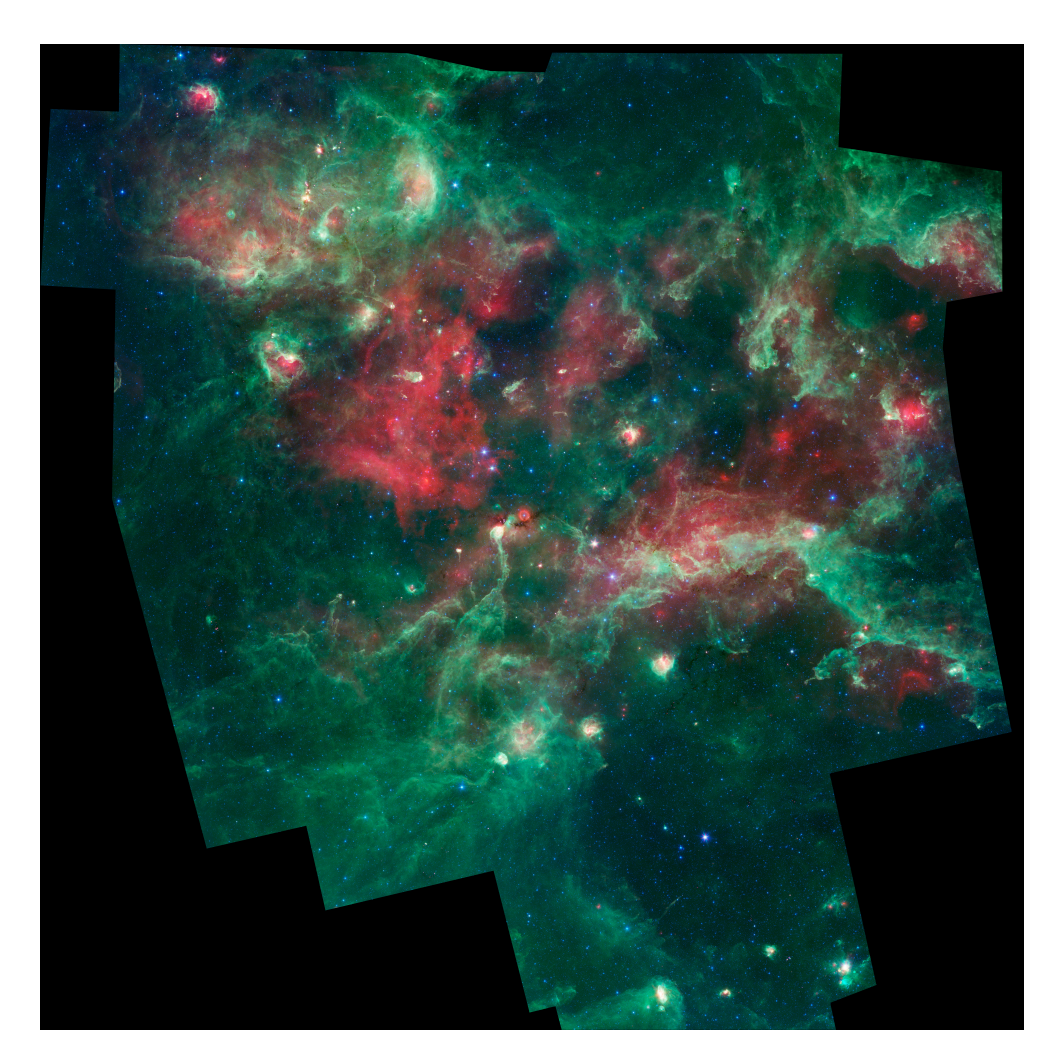


Figure 1.3: Full size mosaic image of the Cygnus-X massive star forming region in the constellation Cygnus, taken with NASA's Spitzer space telescope. The three colours in the image correspond to 3.6/4.5  $\mu m$  (blue), 8  $\mu m$  (green) and 24  $\mu m$  (red). Cool dust and ionised gas can be seen in red. The ionising stars are seen as blue dots as clusters of forming massive stars irradiate their surroundings and sweep up gas and dust into bubbles and pillars. This image fully portrays the violent and chaotic environment of massive star formation. Portions of the cloud have been completely dispersed while filamentary structures are created promoting the further formation of stars, resulting in stars in different stages of their evolution, including young stars with planet-forming disks, deeply embedded embryonic stars and stars in the final stages of their life. Acknowledgement: NASA/JPL-Caltech/Harvard-Smithsonian CfA.

emission. These have masses of a few hundred to a few thousand  $M_{\odot}$ , and will eventually form many massive stars in a clustered manner (Lada & Lada 2003); thus massive protostars are almost exclusively observed to form in clusters. The role of filaments in allowing this kind of clustered star formation may be vital as merging filaments provide regions of very high density (Schneider et al. 2012). Evidence for such intersecting filaments has been seen in the Cygnus-X star forming region (Hennemann et al. 2012), shown in Figure 1.3.

Temperatures in the envelope quickly rise to above 100 K, initiating the onset of the hot molecular core phase (van der Tak 2003; Cesaroni et al. 2005b; Beuther 2006). This phase being the main focus of this thesis, the hot core will be discussed more extensively in its own section below. After the star has evolved enough to produce a high enough EUV flux to ionise hydrogen, it will begin to ionise the surrounding gas forming a very confined hypercompact HII region (Fig 1.4), characterised by broad hydrogen recombination lines (Zinnecker & Yorke 2007). This will continue to expand and evolve to an ultracompact HII region and eventually a classical HII region. During the hypercompact HII region phase, the disk of the massive star is likely still present whereas by the ultracompact HII region phase, the disk has most likely been fully dispersed (Keto 2007; Nielbock et al. 2007).

There are three main models for how massive stars form, and potentially all three contribute to the observed massive stars in the universe. The first is the most similar to the formation of a low mass star, and is called monolithic collapse (Tan & McKee 2003). This involves the collapse of an individual core, and the subsequent build-up of the star through an accretion disk (Yorke & Sonnhalter 2002; Krumholz, Klein & McKee 2005). An alternative way of stellar growth is competitive accretion (Bonnell et al. 1997). In this scenario, specific regions of the stellar cluster are more prone to accreting material depending on the distribution of the stars, therefore stars in these advantageous regions may accrete material easier than their neighbours. This has a feedback loop characteristic to it since, as the star grows, its force of gravitational attraction increases and the advantaged star can accrete still more material with respect to its neighbours. Competitive accretion is also expected to involve an accretion disk. The third process is stellar mergers in which stars collide to form larger mass stars (Bonnell, Bate & Zinnecker 1998). This theory is not as commonly considered as it faces a variety of challenges; most important the pre-requisite of a high stellar density. However it may be the cause of the formation of a very low number of very massive stars.

At first look, low mass and high mass star formation may appear rather similar when considering monolithic collapse, with many of the same emerging global structures, however under the surface there are important details in the physics which significantly distinguish these two evolutionary processes. For example the formation of both types of star most likely involves the role of a disk, however in high mass stars the extreme luminosities involved  $(10^4-10^5 L_{\odot})$  leads to the radiation pressure from massive stars exceeding the gravitational force, which should halt collapse and the subsequent build up of the star (Wolfire & Cassinelli 1986; Zinnecker & Yorke 2007). This high radiation pressure also leads to very strong bipolar stellar winds and outflows which are magneto-centrifugally driven in low mass stars. Furthermore, the high levels of EUV photons photoevaporate the disk early on, whereas in low mass

1.1. STAR FORMATION 9

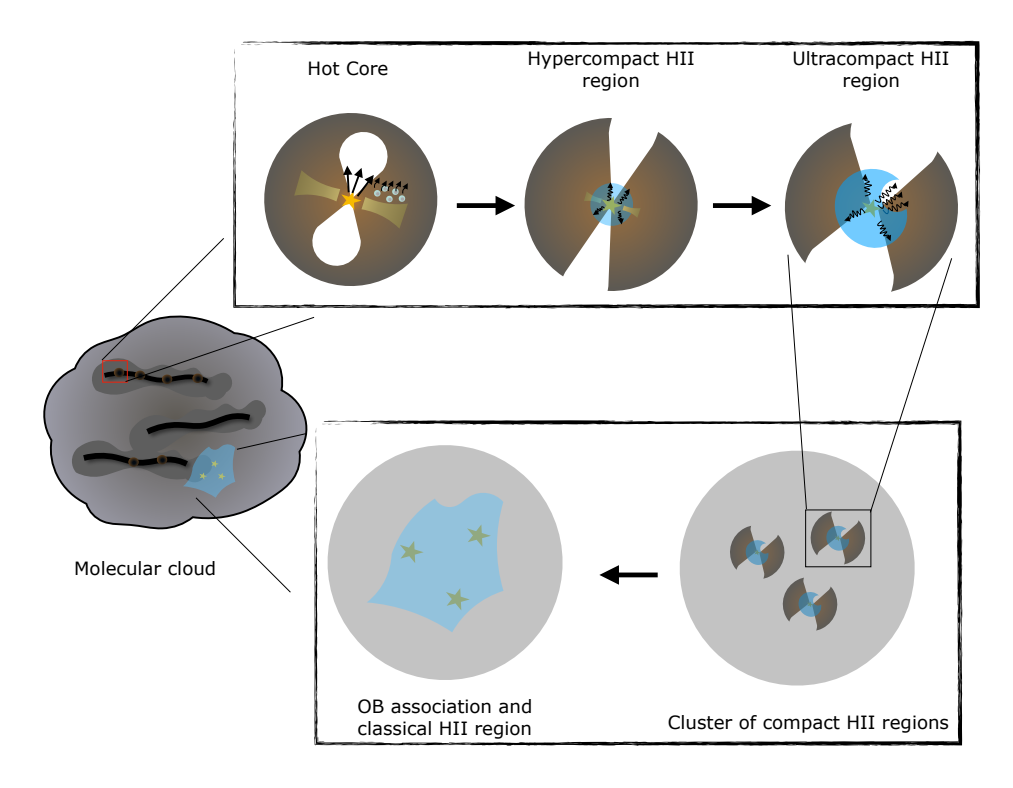


Figure 1.4: Cartoon depicting the evolutionary sequence for the formation of massive stars.

stars this occurs in the disk dispersal phase. The impact of the high flux of ionising photons is not the only source of differences between the two stellar groups, because the ionising photons are able to dissociate  $H_2$  and CO in the nearby environment as well as ionising hydrogen resulting in the formation of HII regions. These complications do not exist in low mass star formation. A particularly striking outcome of this is that ionising radiation from the star can escape through cavities in the polar directions that are blown by these winds resulting in the so-called flashlight effect (Nakano 1989; Yorke & Bodenheimer 1999; Kuiper et al. 2016). Here infrared and UV photons, which exert radiation pressure, interact with the accretion flow through the disk and are absorbed by the innermost region of the disk, the most fundamental zone being the dust sublimation front. This heated region of the disk will then cool through the optically thin layers of the disk photosphere in the vertical direction via the bipolar outflow cavity, and thus the rest of the disk is strongly shielded in the radial direction from the stellar radiation (Kuiper et al. 2010; Tanaka et al. 2016, 2017).

#### Hot Cores

As mentioned above, hot molecular cores are intermediate objects in the high mass star formation process. They can be characterised as regions which are greater than 100 K in temperature, less than 0.1 pc in size, and have densities greater than 10<sup>7</sup> cm<sup>-3</sup> (Kurtz et al. 2000). The temperature and density structure is such that these increase towards the centre of the core, located in a larger scale molecular clump, consistent with these objects being the sites of star formation. Methanol and OH masers are unique to massive star forming regions, and are generally associated with the Hot Core phase, likely probing the sites of disks or outflows, whereas water masers are characteristic of both low and high mass star forming regions. The Hot Core phase has been associated with the disk accretion phase (Patel et al. 2005; Kraus et al. 2010; Moscadelli & Goddi 2014; Johnston et al. 2015; Ilee et al. 2016; Moscadelli et al. 2019; Zapata et al. 2019; Maud et al. 2019), with several disks observed at the centres of hot cores, although to what extent this is the case remains to be established. This is supportive of the core accretion model for massive star formation. There is also evidence that Hot Cores are collapsing strengthening the relation to the disk accretion phase (Hofner, Peterson, & Cesaroni 1999; Osorio et al. 2009; Beltrán et al. 2018).

Another very important feature of hot cores is their chemical diversity with high temperatures providing ideal conditions for the formation of complex organic molecules (COMs). These are defined as molecules with six or more atoms, and many of theses have been detected for the first time towards Hot Cores (Herbst & van Dishoeck 2009). Some COMs are formed on dust grain surfaces in the colder, preceding stages of star formation as ices. Once the Hot Core reaches temperatures of above ~100 K, these ices evaporate leading to a rich gas-phase chemistry where many more COMs are produced with increasing complexity, depicted in Figure 1.4. The high temperatures (100-300 K) allow new energy barriers to be overcome, facilitating chemical reactions that cannot take place in colder environments. The presence of COMs is not unique to high mass objects however, as Hot Cores also have low mass analogues called Hot Corinos (Cazaux et al. 2003; Bottinelli et al. 2004; Ceccarelli 2008), such as the Class 0 binary IRAS 16293-2422.

# 1.2 Chemistry of Circumstellar Disks

Disks associated with Herbig AeBe stars and T-Tauri stars are considered to be externally illuminated, thus the temperature profile of the disk is such that the surface layer of the disk is much hotter than the mid-plane of the disk. Deviations from this scenario come in the form of FU Orionis variables. In these objects very high accretion rates in the disk occur in bursts leading to an inversion of the temperature structure such that the mid-plane is much hotter than the surface, as the disk heating becomes dominated by dissipation of gravitational potential energy. Thus molecular transitions are observed to be in absorption towards these kinds of disks. The result of the temperature stratification of externally illuminated disks is that a chemical stratification also occurs, with different molecular species dominating at different temperatures, and therefore different locations in the disk.

The chemistry of the hot upper layers is controlled by UV and X-ray photons, and in the case of massive stars EUV photons will also contribute. Temperatures exceed 1000 K in both the gas and the dust (although decoupled) making it difficult for most molecules to survive in this region of the disk. Some molecules that can survive are

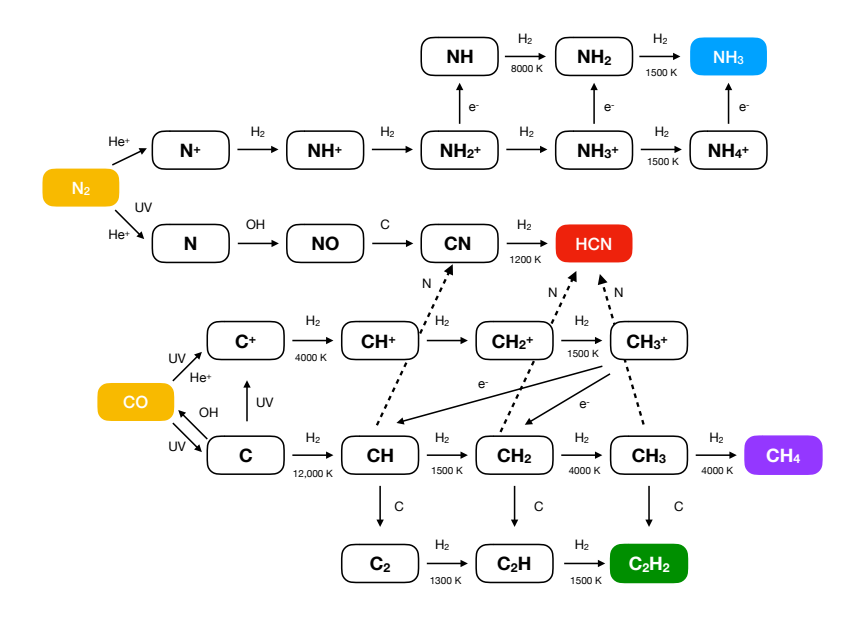


Figure 1.5: Chemical network of the main reactions with high activation energies to produce HCN, C<sub>2</sub>H<sub>2</sub>, CH<sub>4</sub> and NH<sub>3</sub>. The reactions with the highest energy barriers have this quantified where appropriate. Adapted from Bast et al. (2013) and Agúndez et al. (2008).

H<sub>2</sub>, CO, and N<sub>2</sub>, as these molecules form rapidly at high temperatures and are hard to dissociate, meaning that they can self-shield (van Dishoeck & Black 1988; Visser et al. 2009). The rest of the gas will mostly consist of atoms and ions. Close to the mid-plane, the radiation field of the star is strongly attenuated by the upper layers of the disk. Therefore the majority of the gas-phase chemistry will depend on cosmic rays to be triggered. Temperatures are below 100 K in this part of the disk. Cosmic rays can produce H<sub>3</sub><sup>+</sup> and He<sup>+</sup> which can initiate ion-molecule chemistry, as well as a UV field due to the interaction with H<sub>2</sub> molecules. These weak energy sources can further process ices that reside on dust grain mantles to produce species such as NH<sub>3</sub> and CH<sub>4</sub>, as well as more complex species such as CH<sub>3</sub>OH and CH<sub>3</sub>OCH<sub>3</sub> (Öberg et al. 2008; Öberg 2016). Some of the solid-state chemical products from the dark cloud stage preceding the disk stage, as well as gas-phase products from the cloud warm-up stage, may be incorporated into the disk (Visser et al. 2009), however it is possible that the chemistry is reset by accretion shocks as material accretes from the envelope to the disk (Jørgensen, Belloche & Garrod 2020).

The warm region of the disk has temperatures between 100 K and 1000 K and is the production site of simple species such as HCN,  $\rm C_2H_2$ ,  $\rm NH_3$ ,  $\rm CH_4$  and  $\rm H_2O$  in high abundances. In contrast to hot cores,  $\rm CH_3OH$  (Walsh et al. 2016),  $\rm CH_3CN$  (Öberg et al. 2015) and t-HCOOH (Favre et al. 2018) are the only COMs to be detected in disks. This apparent difference may result from chemistry involving evaporating ices inherited from the dark cloud phase and the warm chemistry initiated in the gas phase, or the column densities of COMs in disks may simply be too low for current instrumentation to detect. The UV and X-ray flux from the star allow C and N to

be broken free from the parent bearing species CO and  $N_2$ , which can then react through a network of chemical reactions to form these species outlined in Figure 1.5. The high temperatures facilitate the initial reactions to form C-bearing species from CO, which have very high energy barriers, and HCN,  $C_2H_2$  and  $CH_4$  can be formed.  $CO_2$  may also be produced, however the abundance of this species peaks between 100 K and 200 K because the main reaction to form  $CO_2$  is OH + CO, and OH is driven rapidly into  $H_2O$  at temperatures above 250 K. The high temperatures also allow the reactions of  $CN + H_2$  and  $NH + H_2$  to form HCN and  $NH_3$  respectively. CS is another molecule that can be formed in high abundances in disks (Agúndez et al. 2018).

# 1.3 Absorption Lines at Infrared Wavelengths

### 1.3.1 Ro-vibrational Spectroscopy

Molecular transitions provide an excellent tool for studying star formation, as the discrete frequencies of these transitions allow specific molecules to be uniquely identified. With the large amount of knowledge of the behaviour of astrophysically relevant molecules readily obtained from the highly controlled environment of laboratories here on Earth, molecules can provide information on the physical conditions of star forming regions, as well as on the chemical process taking place.

At mid-infrared wavelengths molecular lines are predominantly due to ro-vibrational transitions. These involve transitions between a rotational level in a certain vibrational level, to a rotational level in another vibrational level, altering the vibrational energy of the molecules. The result is complex spectra such as those illustrated in Figure 1.6. Linear molecules such as CS exhibit a relatively simple spectrum, with lines evenly spaced, whereas non-linear molecules such as  $H_2O$  and  $NH_3$  show complex patterns that are difficult to identify. HCN and  $C_2H_2$  have P, R and Q branches, which are ro-vibrational bands that are formed due to transitions that change rotational quantum number, J, by 1, -1 and 0 respectively.  $H_2O$  and  $NH_3$  are described by quantum numbers J,  $K_a$  and  $K_c$ . The ro-vibrational levels are split into ortho and para states with para states having both  $K_a$  and  $K_c$  odd or even, and ortho states with either  $K_a$  or  $K_c$  odd or even. Transitions between ortho and para states are not allowed, however transitions may occur between two ortho or two para states. The reader is referred to Papousek (1982) and Mihalas (1978) for more information on ro-vibrational spectroscopy and absorption line formation, respectively.

# 1.3.2 Absorption Line Formation

Towards massive protostars ro-vibrational transitions in the infrared are typically seen in absorption against the bright infrared continuum. Thus absorption lines at infrared wavelengths allow for the determination of the physical conditions of these regions. To understand the formation of absorption lines we begin with the absorption coefficient,  $\alpha_{\nu}$ , and its relation to the optical depth,  $\tau_{\nu}$ , of a molecular transition. The absorption coefficient can be defined as such in equation 1.1:

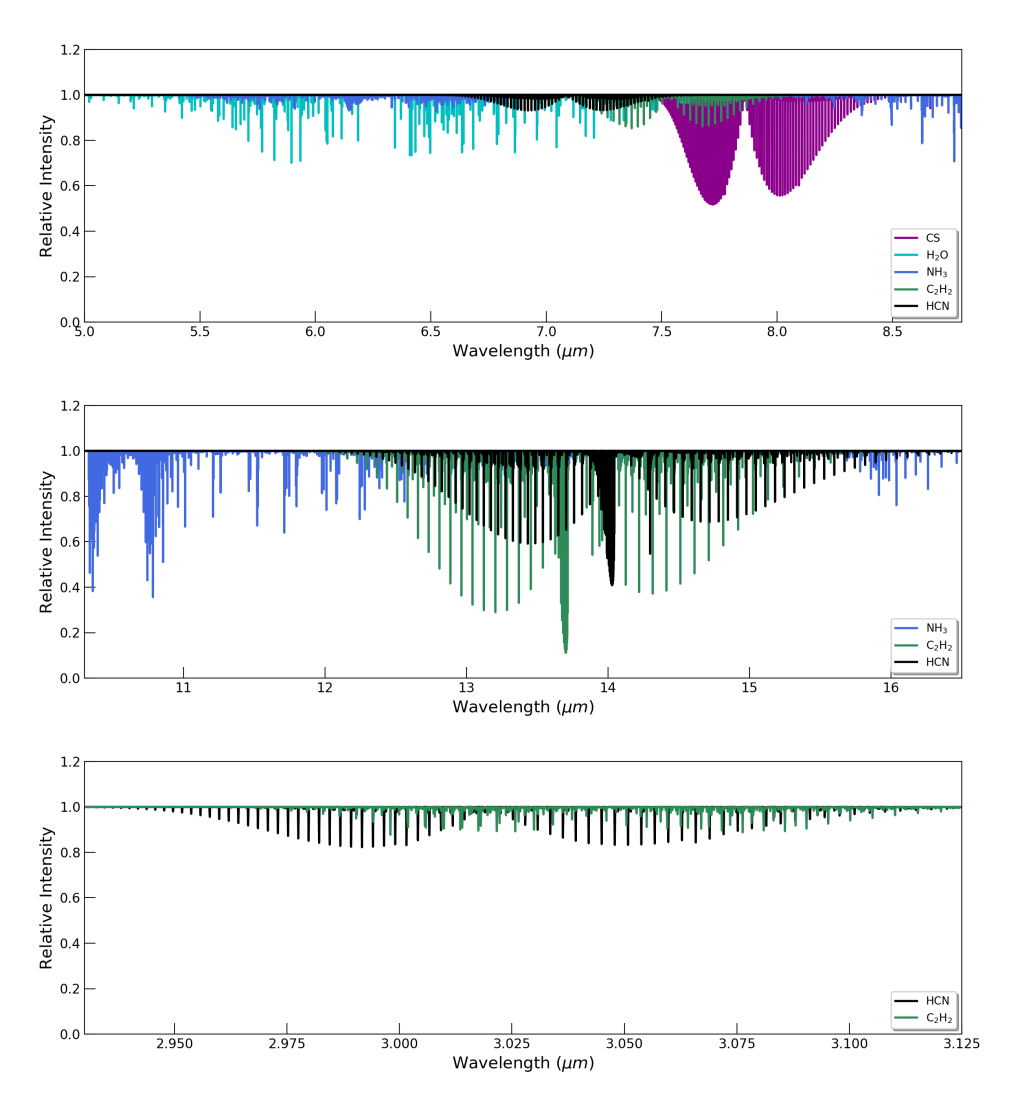


Figure 1.6: Model absorption line spectra of  $\rm H_2O$ , HCN,  $\rm C_2H_2$ , NH<sub>3</sub> and CS at a column density of  $1\times10^{17}$  cm<sup>-2</sup> and a temperature of 500 K. The  $\rm H_2O$  lines are relatively weak compared to the other species, however in practice, these lines are observed to be the strongest due to the large column density in star forming regions ( $10^{18}$  cm<sup>-2</sup>). The bands at 13  $\mu m$  are stronger relative to the bands at other wavelengths for HCN,  $\rm C_2H_2$  and NH<sub>3</sub>.

$$\tau_{\nu} = \int \alpha_{\nu} ds = \int \frac{h\nu}{4\pi} \phi(\nu) (n_u B_{ul} - n_l B_{lu}) ds \tag{1.1}$$

where  $\nu$  is the frequency,  $n_u$  and  $n_l$  are the density of particles in the upper and lower state energy levels respectively,  $B_{ul}$  and  $B_{lu}$  are the Einstein B coefficients, and  $\phi(\nu)$  is the line profile. Under molecular cloud conditions  $\phi(\nu)$  is best described by

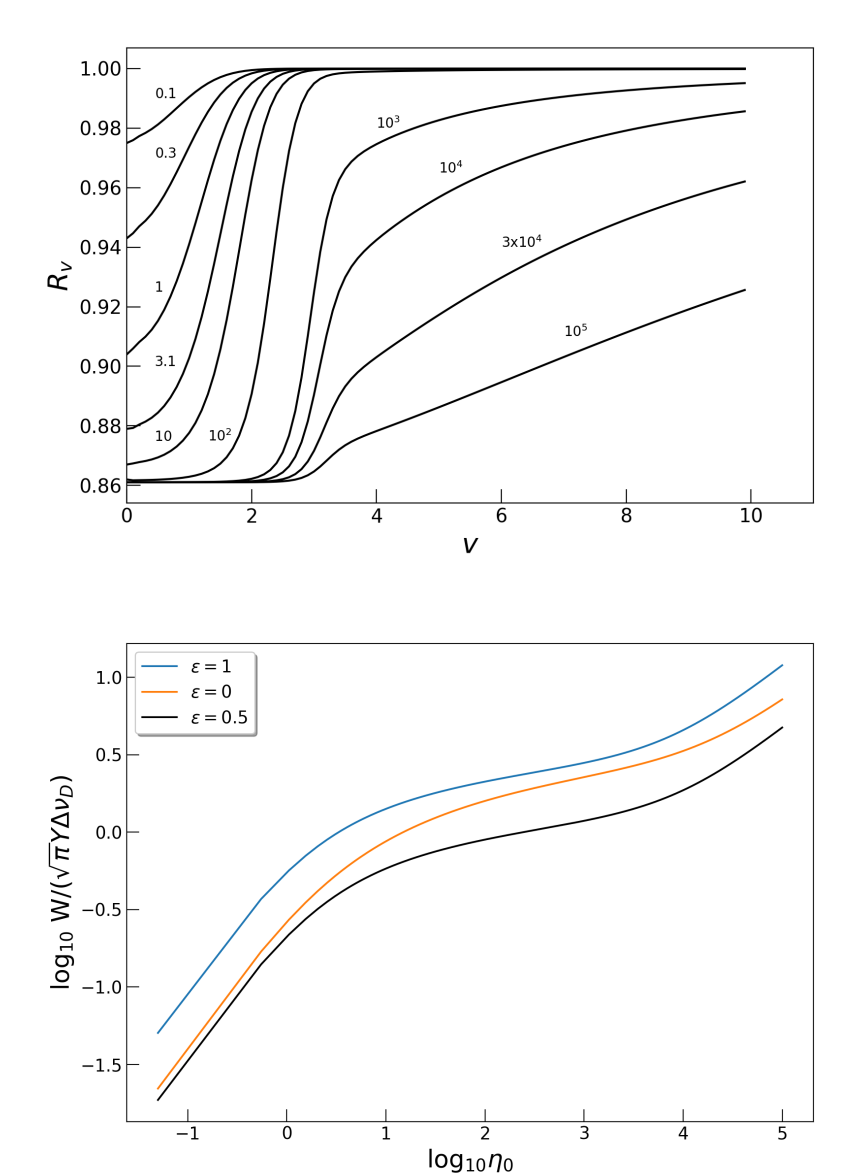


Figure 1.7: top: The calculated profile of an absorption line as a function of the opacity  $\eta_0$ . v is the frequency-parameter describing the Voigt profile, and  $R_v$  is the residual flux of the absorption line, and can be described as 1 - Y, where Y is the line depth. Values for  $\eta_0$  are indicated for the corresponding curves. Taken from Mihalas (1978). bottom: The theoretical curve of growth for three different assumptions of line formation.  $\epsilon$  equal to 1, 0 and 0.5 represents line formation via pure absorption, pure scattering and a combination of the two, respectively (see Appendix of chapter 3 for more details). W is the equivalent width and  $\Delta \nu_D$  the Doppler parameter.

a Voigt profile (a combination of a Lorentzian and Gaussian line profile), however often simply a Gaussian profile is a very good approximation. The relation derived by Einstein for  $B_{ul}$  is:

$$B_{ul} = \frac{A_{ul}c^2}{2h\nu^3} \tag{1.2}$$

and the expression for the level populations in local thermodynamic equilibrium (LTE) is:

$$\frac{n_u}{n_l} = \frac{g_u}{g_l} \exp\left[\frac{-h\nu}{kT_{ex}}\right] \tag{1.3}$$

where  $g_u$  and  $g_l$  are the upper and lower state statistical weights,  $A_{ul}$  is the Einstein A coefficient and  $T_{ex}$  is the excitation temperature. After some simple algebraic manipulation, and integrating over the distance, ds, we arrive at the expression for the optical depth of a line:

$$\tau_{\nu} = \frac{A_{ul}c^2}{8\pi\nu^2} \frac{g_u}{g_l} (1 - e^{-h\nu/kT_{ex}}) \phi(\nu) N_l \tag{1.4}$$

Thus we see that the optical depth is directly proportional to the column density in the lower level of the transition,  $N_l$ . The column density in the lower level of a transition is related to the total column density, N, of a molecule via:

$$N_l = g_l e^{-E_l/kT} \frac{N}{Q(T)} \tag{1.5}$$

where  $E_l$  is the energy of the transition and Q(T) is the partition function at any given temperature. Thus the resulting optical depth will be exponentially dependent on the temperature. The relative intensity is related to the optical depth as  $I = e^{-\tau_{\nu}}$ . Then adopting a line profile, and using the line information from the HITRAN database (Rothman et a. 2013) we can construct synthetic spectra for molecules of interest, such as those shown in Figure 1.6.

In the limit of high optical depth, absorption lines will begin to broaden. When this happens the column density is no longer linearly related to the optical depth, but rather these two parameters become logarithmically related, and equation 1.5 no longer holds. This is a consequence of the Gaussian component of the line profile (for a Voigt profile) becoming saturated, and the strength of the line scales logarithmically with the column density. Eventually the Lorentzian component of the line profile takes over, and the line broadens due to absorption in the wings. The integrated strength will then scale with the square root of the column density (see top panel of Figure 1.7). The behaviour of the transition can be described by the curve of growth, which is a measure of the equivalent width of an absorption line, W, in relation to its opacity,  $\eta_0$ . Examples of the curve of growth are shown in Figure 1.7 for three different types of line formation. The equivalent width of a line is defined as the width of a rectangle that has the height of the continuum and the area of the line profile. For a continuum normalised absorption line the equivalent width of the absorption line will be equal to its area.



Figure 1.8: NASA's SOFIA observatory in full flight with the telescope door open taking data.

Absorbing gas can be seen in the foreground against the infrared continuum source, however the continuum emitting dust and absorbing gas can also be mixed, coming from the same physical space. A consequence of the latter is that an absorption line at a specific wavelength will typically probe the gas to the point where the line plus continuum optical depth becomes equal to 2/3. This follows directly from the Eddington approximation where the temperature equals the effective temperature where the optical depth equals 2/3 (Mihalas 1978). The result is that the absorption lines will probe to varying depths in the gas, leading to discrepancies in the absolute and relative column densities. Furthermore, the simple curve of growth analysis assumes that the absorption coefficient is constant with depth, and ignores any temperature or density gradients in the absorbing gas, which is generally not realistic.

# 1.3.3 Observations of Gas-phase Absorption Lines

This thesis continues a long study of absorption lines towards MYSOs in the infrared regime, presenting results from the first full spectral survey of the 4-13  $\mu m$  wavelength region at high spectral resolution, as well as the first L band observations of organics in MYSOs. By combining ground based surveys from the Infrared Telescope Facility (IRTF) and the Gemini telescope in the L, M and N bands, with SOFIA observations in the 5-8  $\mu m$  region, at high spectral resolution (3-6 km/s), we obtain velocity resolved line profiles of individual ro-vibrational transitions across the mid-IR regime.

The first molecule detected in absorption in the infrared way was CO in the late 1970's towards Orion BN (Hall et al. 1978). This was followed up by Scoville et al. (1983), and Mitchell et al. (1989, 1990) extended this research to a survey of many

different objects. A recurring finding was that CO absorption was observed to be offset in velocity compared to the systemic velocity of the cloud. Velocity differences were generally of the order of 5 km s<sup>-1</sup>, and occurred both in either the blue- or red-shifted directions, depending on the source. Furthermore many different velocity components were detected as well as multiple temperature components, including very hot gas. The first detection of C<sub>2</sub>H<sub>2</sub> in interstellar clouds followed (Lacy et al. 1989), which was shortly succeeded by CH<sub>4</sub> (Lacy et al. 1991), both towards massive protostars. Evans, Lacy & Carr (1991) then detected HCN, C<sub>2</sub>H<sub>2</sub> and NH<sub>3</sub>, again towards Orion, this time in IRc2 and IRc7, with OCS also detected towards IRc2 (Mitchell et al. 1989, 1990; Black et al. 1990; Mitchell et al. 1991).

With the advent of the Infrared Space Observatory (ISO), the possibility to detect H<sub>2</sub>O without interference from the Earth's atmosphere allowed spectral surveys of MYSOs at low spectral resolution (Boonman et al. 2003a; Boonman & van Dishoeck 2003). The first detection of H<sub>2</sub>O in the interstellar medium at infrared wavelengths was towards AFGL 2591, one of the main objects in this thesis (Helmich et al. 1996). Water gas was found to be in absorption, and very abundant in the hot gas close to the protostars. ISO also saw the detection of gas phase CO<sub>2</sub> and SO<sub>2</sub> in the infrared towards a sample of massive protostars (Boonman et al. 2000; Keane et al. 2001; Boonman et al. 2003b), as well as the first interstellar detection of CH<sub>3</sub> (Feuchtgruber et al. 2000). Lahuis & van Dishoeck (2000) detected very hot and abundant HCN and C<sub>2</sub>H<sub>2</sub> in absorption with ISO towards a sample of massive protostars. Boonman et al. (2001) found that sub-mm observations of the high energy J=9-8 rotational lines from the  $\nu_2 = 0$  and  $\nu_2 = 1$  levels of HCN, probed the same gas in emission towards AFGL 2591. The abundance measured was two orders of magnitude higher than the envelope, suggesting a jump in the abundance of HCN in the hot gas very close to the protostar. High spectral resolution cross-echelle spectrographs such as the Texas Echelon Cross Echelle Spectrograph (TEXES; Lacy et al. 2002) improved observations at infrared wavelengths beginning studies at a resolving powers above R=50,000. Knez et al. (2009) detected many species towards NGC 7538 IRS1 with TEXES, including first detections of HNCO and CS in the infrared.

The observation of absorption lines at infrared wavelengths offers many essential differences for studying star forming regions compared to sub-mm emission line studies. Due to the nature of absorption lines, beam size variations with wavelength are not an issue since the beam size is set by the size of the infrared continuum source, the observer only seeing everything along the line of sight between them and the continuum. As a consequence of this, very high spatial resolution is a given. Star forming regions, and particularly circumstellar disks, are very bright at these wavelengths—they are the main infrared continuum source—therefore absorption lines at infrared wavelengths naturally probe material very close to the protostar. A typical observational setting covers 0.2-0.3  $\mu m$ , therefore many lines can be observed in a single setting (Fig 1.6). Finally specific molecules that do not have permanent dipoles, and yet are important members of the organic inventory, are not observable at sub-mm wavelengths but have strong transitions in the infrared (such as CH<sub>4</sub>, C<sub>2</sub>H<sub>2</sub> and CO<sub>2</sub>).

These advantages do not come for free however, and there are several challenges associated with this method (Lacy 2013). In the case that the absorbing gas is physically separated from the emitting dust, if the foreground gas does not fully cover

the continuum, the derived column density of the gas will be underestimated. Along with absorbing material in the foreground, absorbing gas is often found to be mixed with the emitting dust however, leading to radiative transfer effects which complicate the analysis. Furthermore, realistically the continuum source also has a temperature gradient that increases towards the protostar, therefore the dust emission may arise from hotter regions closer to the star than where the gas probes. Finally, observationally, many of these species are very abundant in the Earth's atmosphere, therefore absorption by telluric lines can be difficult to correct for, often resulting in residual absorption features that are hard to distinguish from real features, or removing parts of real features, however large Doppler shifts can mitigate this. Removing the Earth's atmosphere generally involves the use of a featureless star (or standard star) that will then only contain the telluric lines, and this greatly increases observing time. Atmospheric models provide an efficient way to remove the atmosphere from science spectra, often resulting in a better solution.

### 1.4 SOFIA

The Stratospheric Observatory for Infrared Astronomy (SOFIA) is a modified Boeing 747-SP aeroplane that has been adapted to the purpose of infrared astronomy and is a joint project of NASA and the German Aerospace Center (DLR). Within the aircraft is a telescope with a 2.7 m mirror that can be exposed via a door in the side of the plane. SOFIA is unique in the sense that it can fly at altitudes of up to 45,000 ft to take data, however unlike space telescopes, can be continually upgraded and repaired when it lands again. Thus data can be taken at altitudes where transmission through the atmosphere is much better, particularly in the infrared. Figure 1.9 compares the atmospheric transmission at altitudes typical of SOFIA with that of ground based observatories. SOFIA is based at NASA's Armstrong Flight Research Centre in Palmdale California and also in Christchurch International Airport in New Zealand. In this thesis we use the Echelon-cross-Echelle Spectrograph (EXES) on-board SOFIA, making use of the high resolution mode which can achieve a spectral resolution of  $5 \times 10^4$ -1×10<sup>5</sup>. The combination of echelon and echelle gratings as primary and secondary dispersers, respectively, produces spectra that are split into orders, the number of which depends on the spectral resolution mode. EXES operates between 4.5-28.3  $\mu m$  allowing the study of ro-vibrational transitions of many molecules of astrophysical interest.

### 1.4.1 Data Reduction

There are a number of steps required to turn an observation into a usable spectrum. Firstly a flat field is taken and used to correct for unequal spectral and spatial gains as well as calibrating the intensity. The spectrum is also wavelength calibrated using bright sky lines. The removal of sky emission is achieved by nodding either on or off the slit and subtracting each B nod from each A nod. The spectrum must then be extracted from the aperture within a given spatial range of the slit. The various cycles of the observation can then be combined. The final stage in obtaining a complete

1.5. THIS THESIS 19

spectrum is to merge the different Echelle orders, however this requires that the atmosphere has first been removed, either by dividing by a standard star or using an atmospheric model.

### 1.5 This Thesis

With the use of EXES on-board SOFIA to obtain data in the 5-8  $\mu m$  wavelength region, combined with ground based facilities using TEXES to obtain 8-13  $\mu m$ , this thesis presents the first spectral survey of the mid-IR regime of two hot cores, AFGL 2591 and AFGL 2136, at high spectral resolution. iSHELL observations in the L and M bands complete the survey providing much needed information on CO (at high spectral resolution), and also the HCN and  $C_2H_2$  stretching modes at 3  $\mu m$ . The stretching mode of HCN in MonR2 IRS 3 is also analysed. Resolving powers range from 50,000 - 80,000. These targets are very well studied objects at infrared and sub-mm wavelengths.

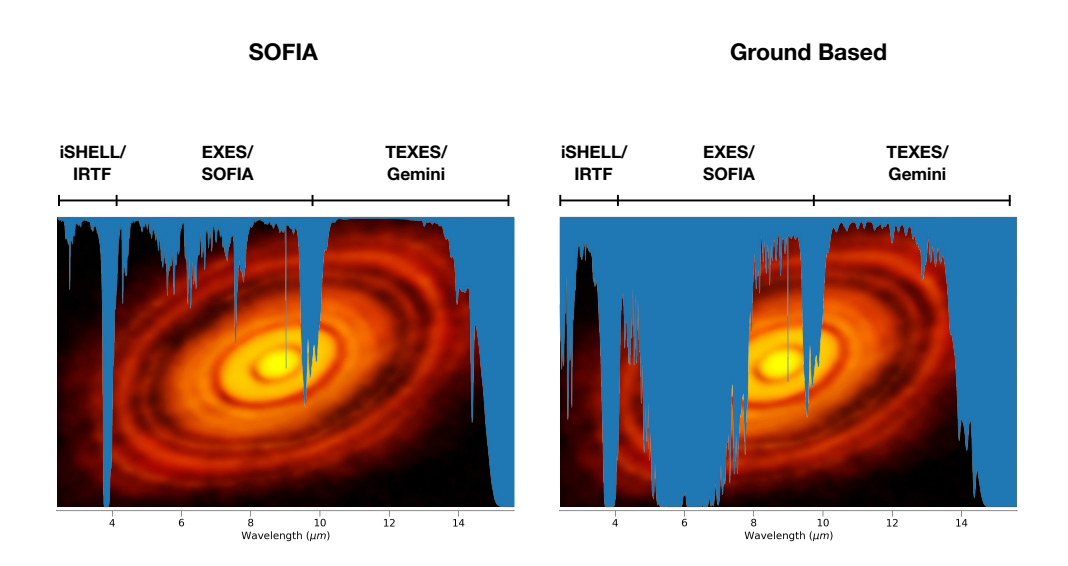


Figure 1.9: Dust continuum emission image of the TTauri disk HL Tau (ALMA Partnership et al. 2015) overlaid with the atmospheric transmission of SOFIA (left) and the IRTF on Mauna Kea (right) in the 3 to 15  $\mu m$  range calculated using the ATRAN model (Lord 1992). Water vapours are 7.6  $\mu m$  and 1.3 mm for SOFIA and IRTF respectively.

Chapter 2 presents the detection of CS with EXES in AFGL 2591 at high spectral resolution, constituting the second detection of CS in this way. These data are complemented by iSHELL observations of CO, and both CS and CO are observed in absorption.  $^{12}$ CO lines are highly optically thick and saturated, therefore we limit the discussion to the optically thin isotopologue  $^{13}$ CO, which shows five blended velocity components. We discern two temperature components in CO at the velocity of CS, where a narrow component is superimposed on a broad underlying component, which disappears above J=6. The temperature of the hot CO component is in agreement with the temperature of CS, and is  $\sim$ 700 K. The column density, and abundance with respect to CO, of CS is two orders of magnitude higher than derived from sub-mm observations which detect CS in emission. This points towards a large reservoir of warm sulphur-bearing gas that is not detectable at sub-mm wavelengths, which might help alleviate the low fraction of accounted-for sulphur in dense regions.

Chapter 3 expands the detection of CS in AFGL 2591 to the other simple organics detected in the spectral survey including HCN,  $C_2H_2$  and  $NH_3$ , as well as the detection of all these species in AFGL 2136. All species are observed in absorption and derived temperatures are high (400-700 K). Column density variations are observed in HCN and  $C_2H_2$  with wavelength between vibrational bands that trace the same lower level, where the column at 13  $\mu m$  is a factor of 4-10 lower than the column at 7  $\mu m$ . Furthermore ortho-to-para ratios of  $C_2H_2$  are found to be below the expected value of 3 for a hot gas formation. Supplementary data in the L-band at 3  $\mu m$  for AFGL 2591 find HCN and  $C_2H_2$  in emission. The mid-IR continuum of these two sources originates in a circumstellar disk (Monnier et al. 2009; Frost et al. 2021), therefore we associate the absorbing gas to arise from the disk. We develop a model based on stellar atmosphere theory to account for the temperature gradient in the disk, which is heated from the mid-plane by viscous processes resulting in a temperature gradient that decreases with scale height. We find that the disk model can account for all of the above observational results.

Chapter 4 extends the discussion to H<sub>2</sub>O, with hundreds of absorption lines being detected in both AFGL 2591 and AFGL 2136 from the v=1-0 and v=2-1 bands. Two velocity components are observed in each source. A rotation diagram analysis shows large scatter as lines with high opacity are underestimated compared to low opacity ones. We find that absorption lines saturate at non-zero flux, a direct prediction of the stellar atmosphere model developed in chapter 3. We therefore carry out a curve of growth analysis in this regime, and find that lines with high opacity have transitioned onto the logarithmic part of the curve of growth. The temperatures derived are of the order 400-600 K. The model of an absorbing slab of gas associated with foreground absorption is found to be incompatible with the results; namely the absence of H<sub>2</sub>O emission lines, chemical abundance ratios and unexpected covering factors. The internally heated disk model also has challenges as absorption lines are offset in velocity from the cloud and line widths are narrower than would be expected based on a disk origin, requiring a specific geometry. A velocity gradient is observed with opacity in AFGL 2591 indicative of a disk wind along the observer's line of sight. We conclude that the disk model best explains all of the observational results, including the other species detected.

Chapter 5 presents the detections, in the 3  $\mu m$  spectral window, of HCN towards the high mass protostar MonR2 IRS 3 in emission, and HCN and C<sub>2</sub>H<sub>2</sub> towards AFGL 2136 in absorption. MonR2 IRS 3 is a binary, and our observations allow us to separate the contributions from each source in the binary. HCN is confidently detected in MonR2 IRS 3A and tentatively detected in MonR2 IRS 3B. A rotation diagram analysis reveals hot gas associated in velocity with the red-shifted emission feature of P-cygni profiles seen up to high J levels (J=26) in CO. We attribute the HCN emission either to the back-side of an expanding shell of gas that is moving away from the observer, or to the upper layers of a circumstellar disk photosphere. We explore two options for the absorption lines of AFGL 2136: a foreground absorbing slab model and an internally heated circumstellar disk. For the foreground model, partial covering of the continuum source at 13  $\mu m$  must be invoked in order to explain the equivalent widths, with a covering factor 0.3 of that at 3 and 7  $\mu m$ . An important conclusion of this model is that HCN and  $C_2H_2$  must cover the source more than  $H_2O$ . For the disk model, consistent physical conditions are measured across all wavelengths for HCN, however C<sub>2</sub>H<sub>2</sub> shows a trend of increasing temperature/abundance with decreasing wavelength, indicative of a radial abundance gradient. Both of these sources differ from AFGL 2591 in that no P-Cygni profiles are observed towards AFGL 2591 or AFGL 2136, and AFGL 2591 and MonR2 IRS 3 show emission lines rather than absorption lines.

# 1.6 Future Outlook

The detection of hundreds of ro-vibratioanl transitions towards massive protostars offers the potential to study in detail the physical structure of the inner regions of MYSOs, offering insights that are not possible with sub-mm astronomy. The lack of spatial information (or difficulty in extracting it) in absorption studies presents a challenge in interpreting the results, however, and for that reason very high spatial resolution observations with sub-mm interferometers such as the Atacama Large Millimetre Array (ALMA) are extremely useful in complementing these studies. A particular example is the detection and velocity mapping of the Keplerian disk of AFGL 2136 seen in vibrationally excited  $H_2O$  emission with ALMA (Maud et al. 2019). The James Webb Space Telescope (JWST) will allow the opportunity to study low mass objects at infrared wavelengths due to the high sensitivity, a current limitation to SOFIA studies. The absence of a high resolution spectrometer on JWST means that this thesis will be essential in providing a benchmark for interpreting the lower spectral resolution data, as kinematic information of the different molecular species will not be available. The Mid-Infrared E-ELT Imager and Spectrograph (METIS) on the Extremely Large Telescope (ELT), and NASA's distant future mission Origins Space Telescope, will allow for velocity resolved studies at high sensitivity and will greatly expand this work to fainter high and low mass protostars. This will give the opportunity to determine whether absorption lines are also common in deeply embedded low mass disks, or if this is a characteristic unique to high mass objects,

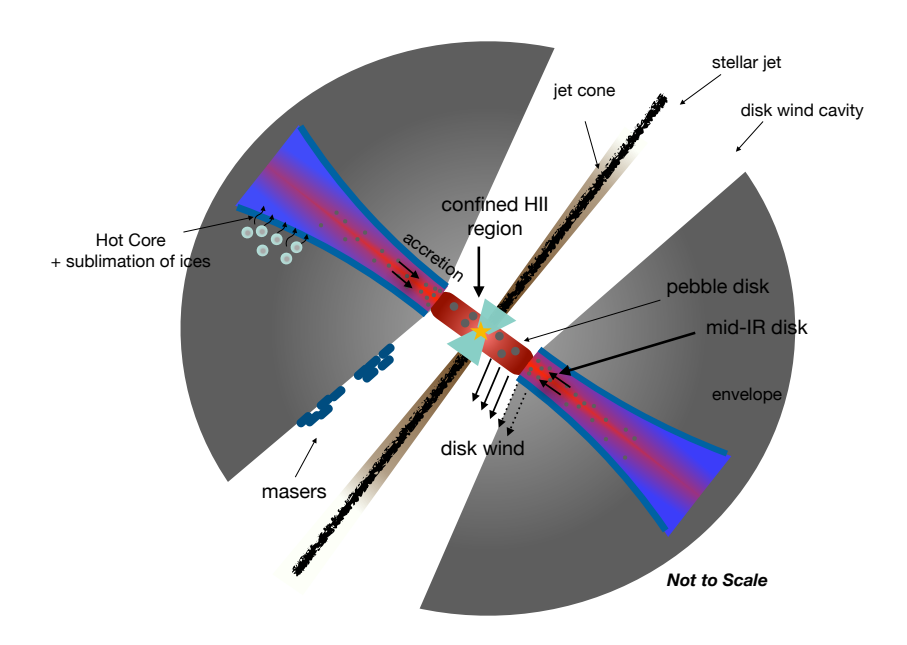


Figure 1.10: Cartoon illustration of the potential environment of MYSOs, taken from chapter 4 of this thesis.

and to understand the different heating mechanisms involved. In the earliest stages of disk evolution of low/intermediate mass stars, we expect that the disk will also be internally heated when the accretion rate is high and stellar luminosity low. Next generation telescopes will help to answer whether this is true or not. Observations of mid-IR absorption lines towards many class 0 disks would be a step toward solidifying this hypothesis, as for now only a few low mass sources show mid-IR absorption lines, which are believed to be due to a rare viewing angle (Gibb et al. 2007; Lahuis et al. 2006; Najita et al. 2021).

On the other side of the coin, of particular importance is the development of theoretical models which are necessary to establish what the temperature and density structures are for disks that are heated internally by viscous dissipation. The complex environment depicted in Figure 1.10 for a MYSO suggests many different physical components that can be modelled and constrained with observations. In this picture, strong winds close to the protostar carve out cavities through which radiation can escape via the flashlight effect, thus shielding the disk from stellar radiation. These winds also excavate the inner disk of small grains, extending the mid-IR continuum origin further out in the disk. From a chemical perspective, chemical models will have to explore what the dominant routes are towards molecules such as HCN and  $C_2H_2$  in these disks, in particular if there are no UV photons available to break carbon out of CO and nitrogen out of  $N_2$ .